GET3D: A Generative Model of High Quality 3D Textured Shapes Learned from Images

Anonymous Author(s)
Affiliation
Address
email

Abstract

As several industries are moving towards modeling massive 3D virtual worlds, the need for content creation tools that can scale in terms of the quantity, quality, and diversity of 3D content is becoming evident. In our work, we aim to train performant 3D generative models that synthesize textured meshes which can be directly consumed by 3D rendering engines, thus immediately usable in downstream applications. Prior works on 3D generative modeling either lack geometric details, are limited in the mesh topology they can produce, typically do not support textures, or utilize neural renderers in the synthesis process, which makes their use in common 3D software non-trivial. In this work, we introduce GET3D, a **G**enerative model that directly generates **E**xplicit **T**extured **3D** meshes with complex topology, rich geometric details, and high fidelity textures. We bridge recent success in the differentiable surface modeling, differentiable rendering as well as 2D Generative Adversarial Networks to train our model from 2D image collections. GET3D is able to generate high-quality 3D textured meshes, ranging from cars, chairs, animals, motorbikes and human characters to buildings, achieving significant improvements over previous methods.

1 Introduction

Diverse, high-quality 3D content is becoming increasingly important for several industries, including gaming, robotics, architecture, and social platforms. However, manual creation of 3D assets is very time-consuming and requires specific technical knowledge as well as artistic modeling skills. One of the main challenges is thus scale – while one can find 3D models on 3D marketplaces such as Turbosquid [4] or Sketchfab [3], creating many 3D models to, say, populate a game or a movie with a crowd of characters that all look different still takes a significant amount of artist time.

To facilitate the content creation process and make it accessible to a variety of (novice) users, generative 3D networks that can produce high-quality and diverse 3D assets have recently become an active area of research [5, 13, 36, 39, 46, 54, 58, 51]. However, to be practically useful for current real-world applications, 3D generative models should ideally fulfill the following requirements: **(a)** They should have the capacity to generate shapes with detailed geometry and arbitrary topology, **(b)** The output should be a textured mesh, which is a primary representation used by standard graphics software packages such as Blender [14] and Maya [1], and **(c)** We should be able to leverage 2D images for supervision, as they are more widely available than explicit 3D shapes.

Prior work on 3D generative modeling has focused on subsets of the above requirements, but no method to date fulfills all of them (Tab. 1). For example, methods that generate 3D point clouds [5, 54, 58] typically do not produce textures and have to be converted to a mesh in post-processing.

Submitted to 36th Conference on Neural Information Processing Systems (NeurIPS 2022). Do not distribute.

Method	Application	Representation	Supervision	Textured mesh	Arbitrary topology
OccNet [36]	3D generation	Implicit	3D	✗	✓
PointFlow [54]	3D generation	Point cloud	3D	✗	✓
Texture3D [46]	3D generation	Mesh	2D	✓	✗
StyleNerf [21]	3D-aware NV	Neural field	2D	✗	✓
EG3D [8]	3D-aware NV	Neural field	2D	✗	✓
PiGAN [7]	3D-aware NV	Neural field	2D	✗	✓
GRAF [50]	3D-aware NV	Neural field	2D	✗	✓
Ours	3D generation	Mesh	2D	✓	✓

Table 1: Comparison with prior works. (NV: Novel view synthesis.)

Methods generating voxels often lack geometric details and do not produce texture [53, 18, 23, 33]. Generative models based on neural fields [36, 13] focus on extracting geometry but disregard texture. Most of these also require explicit 3D supervision. Finally, methods that directly output textured 3D meshes [47, 46] typically require pre-defined shape templates and cannot generate shapes with complex topology and variable genus.

Recently, rapid progress in neural volume rendering [38] and 2D Generative Adversarial Networks (GANs) [29, 30, 28, 25, 45] has led to the rise of 3D-aware image synthesis [7, 50, 8, 42, 44, 21]. However, this line of work aims to synthesize multi-view consistent images using neural rendering in the synthesis process and does not guarantee that meaningful 3D shapes can be generated. While a mesh can potentially be obtained from the underlying neural field representation using the marching cube algorithm [32], extracting the corresponding texture is non-trivial.

In this work, we introduce a novel approach that aims to tackle all the requirements of a practically useful 3D generative model. Specifically, we propose GET3D, a **G**enerative model for 3D shapes that directly outputs **E**xplicit **T**extured **3D** meshes with high geometric and texture detail and arbitrary mesh topology. In the heart of our approach is a generative process that utilizes a differentiable *explicit* surface extraction method [51] and a differentiable rendering technique [40, 31]. The former enables us to directly optimize and output textured 3D meshes with arbitrary topology, while the latter allows us to train our model with 2D images, thus leveraging powerful and mature discriminators developed for 2D image synthesis. Since our model directly generates meshes and uses a highly efficient (differentiable) graphics renderer, we can easily scale up our model to train with image resolution as high as 1024×1024, allowing us to learn high-quality geometric and texture details.

We demonstrate state-of-the-art performance for unconditional 3D shape generation on multiple categories with complex geometry from ShapeNet [9], Turbosquid [4] and Renderpeople [2], such as chairs, motorbikes, cars, human characters, and buildings. With explicit mesh as output representation, GET3D is also very flexible and can easily be adapted to other tasks, including: **(a)** learning to generate decomposed material and view-dependent lighting effects using advanced differentiable rendering [12], without supervision, **(b)** text-guided 3D shape generation using CLIP [49] embedding.

2 Related Work

We review recent advances in 3D generative models for geometry and appearance, as well as 3D-aware generative image synthesis.

3D Generative Models In recent years, 2D generative models have achieved photorealistic quality in high-resolution image synthesis [29, 30, 28, 45, 25, 17, 15]. This progress has also inspired research in 3D content generation. Early approaches aimed to directly extend the 2D CNN generators to 3D voxel grids [53, 18, 23, 33], but the high memory footprint and computational complexity of 3D convolutions hinder the generation process at high resolution. As an alternative, other works have explored point cloud [5, 54, 58, 39], implicit [36, 13], or octree [26] representations. However, these works focus mainly on generating geometry and disregard appearance. Their output representations also need to be post-processed to make them compatible with standard graphics engines.

More similar to our work, Textured3DGAN [47, 46] and DIBR [11] generate textured 3D meshes, but they formulate the generation as a deformation of a template mesh, which prevents them from generating complex topology or shapes with varying genus, which our method can do. PolyGen [41] and SurfGen [34] can produce meshes with arbitrary topology, but do not synthesize textures.

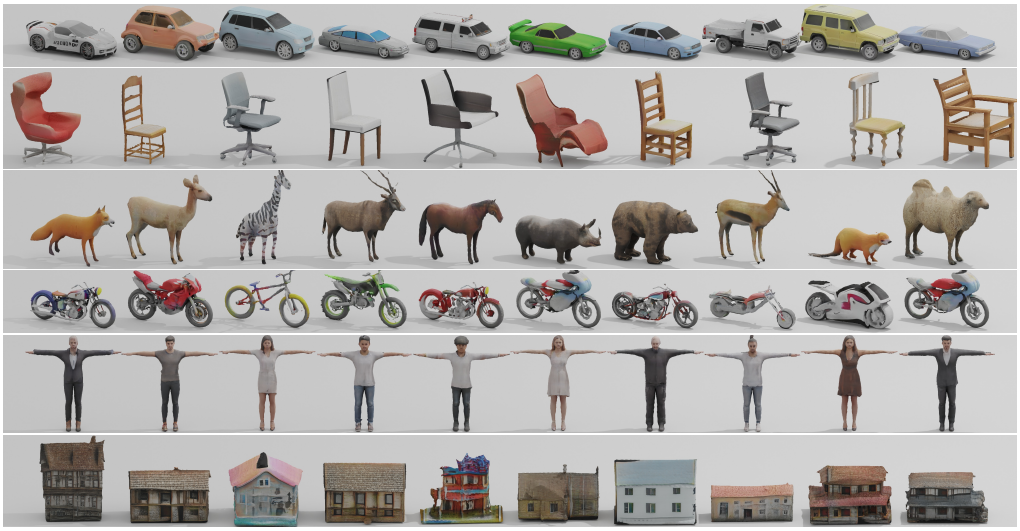

Figure 1: We export our **generated shapes** into Blender. GET3D is able to generate diverse shapes with arbitrary topology, high quality geometry and texture.

3D-Aware Generative Image Synthesis Inspired by the success of neural volume rendering [38] and implicit representations [36, 13], recent work started tackling the problem of 3D-aware image synthesis [7, 50, 42, 22, 21, 59, 8, 44]. However, neural volume rendering networks are typically slow to query, leading to long training times [7, 50], and generate images of limited resolution. GIRAFFE [42] and StyleNerf [21] improve the training and rendering efficiency by performing neural rendering at a lower resolution and then upsampling the results with a 2D CNN. However, the performance gain comes at the cost of a reduced multi-view consistency. By utilizing a dual discriminator, EG3D [8] can partially mitigate this problem. Nevertheless, extracting a textured surface from methods that are based on neural rendering is a non-trivial endeavor. In contrast, GET3D directly outputs textured 3D meshes that can be readily used in standard graphics engines.

3 Method

We now present our GET3D framework for synthesizing textured 3D shapes. Our generation process is split into two parts: a geometry branch, which differentiably outputs a surface mesh of arbitrary topology, and a texture branch that produces a texture field that can be queried at the surface points to produce colors or can be extended to other surface properties such as material (Sec. 4.3.1). During training, an efficient differentiable rasterizer is utilized to render the resulting textured mesh into 2D high-resolution images. The entire process is differentiable, allowing for adversarial training from images (with masks indicating an object of interest) by propagating the gradients from the 2D discriminator to both generator branches. Our model is illustrated in Fig. 2. In the following, we first introduce our 3D generator in Sec 3.1, before proceeding to the differentiable rendering and loss functions in Sec 3.2.

3.1 Generative Model of 3D Textured Meshes

We aim to learn a 3D generator $M, E = G(\mathbf{z})$ to map a sample from a Gaussian distribution $\mathbf{z} \in \mathcal{N}(0, \mathbf{I})$ to a mesh M with texture E.

Since the same geometry can have different textures, and the same texture can be applied to different geometries, we sample two random input vectors $\mathbf{z}_1 \in \mathbb{R}^{512}$ and $\mathbf{z}_2 \in \mathbb{R}^{512}$. Following StyleGAN [29, 30, 28], we then use non-linear mapping networks f_{geo} and f_{tex} to map $\mathbf{z}_1$ and $\mathbf{z}_2$ to intermediate latent vectors $\mathbf{w}_1 = f_{\text{geo}}(\mathbf{z}_1)$ and $\mathbf{w}_2 = f_{\text{tex}}(\mathbf{z}_2)$ which are further used to produce *styles* that control the generation of 3D shapes and texture, respectively. We formally introduce the generator for geometry in Sec. 3.1.1 and the texture generator in Sec. 3.1.2.

3.1.1 Geometry Generator

We design our geometry generator to incorporate DMTet [51], a recently proposed differentiable surface representation. DMTet represents geometry as a signed distance field (SDF) defined on a deformable tetrahedral grid [20], from which the surface can be differentiably recovered through marching tetrahedra [16]. Deforming the grid by moving its vertices results in a better utilization

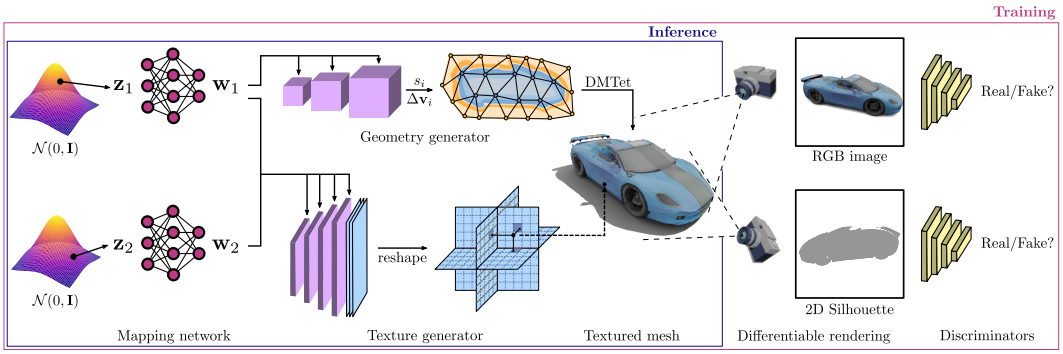

Figure 2: Overview of **GET3D:** We generate a 3D SDF and a texture field via two latent codes. We utilize DMTet [51] to extract a 3D surface mesh from the SDF, and query the texture field at surface points to get colors. We train with adversarial losses defined on 2D images. In particular, we use a rasterization-based differentiable renderer [31] to obtain RGB images and silhouettes. We utilize two 2D discriminators, each on RGB image, and silhouette, respectively, to classify whether the inputs are real or fake. The whole model is end-to-end trainable.

of its resolution. By adopting DMTet for surface extraction, we can produce explicit meshes with arbitrary topology and genus. We next provide a brief summary of DMTet and refer the reader to the original paper for further details.

Let (V_T, T) denote the full 3D space that the object lies in, where V_T are the vertices in the tetrahedral grid T. Each tetrahedron $T_k \in T$ is defined using four vertices $\{\mathbf{v}_{a_k}, \mathbf{v}_{b_k}, \mathbf{v}_{c_k}, \mathbf{v}_{d_k}\}$, with $k \in \{1, \ldots, K\}$, where K is the total number of tetrahedra, and $\mathbf{v}_{i_k} \in V_T, \mathbf{v}_{i_k} \in \mathbb{R}^3$. In addition to its 3D coordinates, each vertex $\mathbf{v}_i$ contains the SDF value $s_i \in \mathbb{R}$ and the deformation $\Delta \mathbf{v}_i \in \mathbb{R}^3$ of the vertex from its initial canonical coordinate. This representation allows recovering the explicit mesh through differentiable marching tetrahedra [51], where SDF values in continuous space are computed by a barycentric interpolation of their value s_i on the deformed vertices $\mathbf{v}'_i = \mathbf{v}_i + \Delta \mathbf{v}_i$.

Network Architecture We map $\mathbf{w}_1 \in \mathbb{R}^{512}$ to SDF values and deformations at each vertex $\mathbf{v}_i$ through a series of conditional 3D convolutional and fully connected layers. Specifically, we first use 3D convolutional layers to generate a feature volume conditioned on $\mathbf{w}_1$. We then query the feature at each vertex $\mathbf{v}_i \in V_T$ using trilinear interpolation and feed it into MLPs that outputs the SDF value s_i and the deformation $\Delta \mathbf{v}_i$. In cases where modeling at a high-resolution is required (e.g. motorbike with thin structures in the wheels), we further use volume subdivision following [51].

Differentiable Mesh Extraction After obtaining s_i and $\Delta \mathbf{v}_i$ for all the vertices, we use the differentiable marching tetrahedra algorithm to extract the explicit mesh. Marching tetrahedra determines the surface topology within each tetrahedron based on the signs of s_i. In particular, a mesh face is extracted when $\text{sign}(s_i) \neq \text{sign}(s_j)$, where i, j denotes the indices of vertices in the edge of tetrahedron, and the vertices $\mathbf{m}_{i,j}$ of that face are determined by a linear interpolation as $\mathbf{m}_{i,j} = \frac{\mathbf{v}'_i s_j - \mathbf{v}'_j s_i}{s_j - s_i}$. Note that the above equation is only evaluated when $s_i \neq s_j$, thus it is differentiable, and the gradient from $\mathbf{m}_{i,j}$ can be back-propagated into the SDF values s_i and deformations $\Delta \mathbf{v}_i$. With this representation, the shapes with arbitrary topology can easily be generated by predicting different signs of s_i.

3.1.2 Texture Generator

Directly generating a texture map consistent with the output mesh is not trivial, as the generated shape can have an arbitrary genus and topology. We thus parameterize the texture as a texture field [43]. Specifically, we model the texture field with a function f_t that maps the 3D location of a surface point $\mathbf{p} \in \mathbb{R}^3$, conditioned on the $\mathbf{w}_2$, to the RGB color $\mathbf{c} \in \mathbb{R}^3$ at that location. Since the texture field depends on geometry, we additionally condition this mapping on the geometry latent code $\mathbf{w}_1$, such that $\mathbf{c} = f_t(\mathbf{p}, \mathbf{w}_1 \oplus \mathbf{w}_2)$, where $\oplus$ denotes concatenation.

Network Architecture We represent our texture field using a tri-plane representation, which is efficient and expressive in reconstructing 3D objects [48] and generating 3D-aware images [8] . Specifically, we follow [8, 30] and use a conditional 2D convolutional neural network to map the latent code $\mathbf{w}_1 \oplus \mathbf{w}_2$ to three axis-aligned orthogonal feature planes of size $N \times N \times (C \times 3)$, where $N = 256$ denotes the spatial resolution and $C = 32$ the number of channels. Given the feature planes, the feature vector $\mathbf{f}^t \in \mathbb{R}^{32}$ of a surface point $\mathbf{p}$ can be recovered as $\mathbf{f}^t = \sum_e \rho(\pi_e(\mathbf{p}))$, where $\pi_e(\mathbf{p})$

is the projection of the point $\mathbf{p}$ to the feature plane e and $\rho(\cdot)$ denotes bilinear interpolation of the features. An additional fully connected layer is then used to map the aggregated feature vector $\mathbf{f}^t$ to the RGB color $\mathbf{c}$. Note that, different from other works on 3D-aware image synthesis [8, 21, 7, 50] that also use a neural field representation, we only need to sample the texture field at the locations of the surface points (as opposed to dense samples along a ray). This greatly reduces the computational complexity for rendering high-resolution images and guarantees to generate multi-view consistent images by construction.

3.2 Differentiable Rendering and Training

In order to supervise our model during training, we draw inspiration from Nvdiffrec [40] that performs multi-view 3D object reconstruction by utilizing a differentiable renderer. Specifically, we render the extracted 3D mesh and the texture field into 2D images using a differentiable renderer [31], and supervise our network with a 2D discriminator, which tries to distinguish the image from a real object or rendered from the generated object.

Differentiable Rendering We assume that the camera distribution $\mathcal{C}$ that was used to acquire the images in the dataset is known. To render the generated shapes, we randomly sample a camera c from $\mathcal{C}$, and utilize a highly-optimized differentiable rasterizer Nvdiffrast [31] to render the 3D mesh into a 2D silhouette as well as an image where each pixel contains the coordinates of the corresponding 3D point on the mesh surface. These coordinates are further used to query the texture field to obtain the RGB values. Since we operate directly on the extracted mesh, we can render high-resolution images with high efficiency, allowing our model to be trained with image resolution as high as 1024×1024.

Discriminator & Objective We train our model using an adversarial objective. We adopt the discriminator architecture from StyleGAN [29], and use the same non-saturating GAN objective with R1 regularization [35]. We empirically find that using two separate discriminators, one for RGB images and another one for silhouettes, yields better results than a single discriminator operating on both. Let D_x denote the discriminator, where x can either be an RGB image or a silhouette. The adversarial objective is then be defined as follows:

$$L(D_x, G) = \mathbb{E}_{\mathbf{z}\in\mathcal{N},c\in\mathcal{C}}[g(D_x(R(G(\mathbf{z}), c)))] + \mathbb{E}_{I_x\in p_x}[g(-D_x(I_x)) + \lambda||\nabla D_x(I_x)||_2^2], \tag{1}$$

where $g(u)$ is defined as $g(u) = -\log(1+\exp(-u))$, p_x is the distribution of real images, R denotes rendering, and λ is a hyperparameter. Since R is differentiable, the gradients can be backpropagated from 2D images to our 3D generators.

Regularization To remove internal floating faces that are not visible in any of the views, we further regularize the geometry generator with a cross-entropy loss defined between the SDF values of the neighboring vertices [40]:

$$L_{\text{reg}} = \sum_{i,j\in\mathbb{S}_e} H\left(\sigma(s_i), \text{sign}\left(s_j\right)\right) + H\left(\sigma(s_j), \text{sign}\left(s_i\right)\right), \tag{2}$$

where H denotes binary cross-entropy loss and σ denotes the sigmoid function. The sum in Eq. 2 is defined over the set of unique edges $\mathbb{S}_e$ in the tetrahedral grid, for which $\text{sign}(s_i) \neq \text{sign}(s_j)$.

The overall loss function is then defined as:

$$L = L(D_{\text{rgb}}, G) + L(D_{\text{mask}}, G) + \mu L_{\text{reg}}, \tag{3}$$

where μ is a hyperparameter that controls the level of regularization.

4 Experiments

We conduct extensive experiments to evaluate our model. We first compare the quality of the 3D textured meshes generated by GET3D to the existing methods using the ShapeNet [9] and Turbosquid [4] datasets. Next, we ablate our design choices in Sec. 4.2. Finally, we demonstrate the flexibility of GET3D by adapting it to downstream applications in Sec. 4.3. Additional experimental results and implementation details are provided in Appendix.

Category	Method	COV (%, ↑)		MMD (↓)		FID (↓)	
		LFD	CD	LFD	CD	Ori	3D
Car	PointFlow [54]	51.91	57.16	1971	0.82	-	-
	OccNet [36]	27.29	42.63	1717	**0.61**	-	-
	Pi-GAN [7]	0.82	0.55	6626	25.54	52.82	104.29
	GRAF [50]	1.57	1.57	6012	10.63	49.95	52.85
	EG3D [8]	60.16	49.52	1527	0.72	15.52	21.89
	Our	**66.78**	**58.39**	**1491**	0.71	**10.25**	**10.25**
	Our+Subdiv.	62.48	55.93	1553	0.72	12.14	12.14
Chair	PointFlow [54]	49.58	**71.87**	3755	**3.03**	-	-
	OccNet [36]	61.10	67.13	3494	3.98	-	-
	Pi-GAN [7]	53.76	39.65	4092	6.65	65.70	120.53
	GRAF [50]	50.23	39.28	4055	6.80	43.82	61.63
	EG3D [8]	58.31	50.14	3444	4.72	38.87	46.06
	Our	69.08	69.91	3167	3.72	23.28	23.28
	Our+Subdiv.	**71.59**	70.84	**3163**	3.95	**23.17**	**23.17**

Category	Method	COV (%, ↑)		MMD (↓)		FID (↓)	
		LFD	CD	LFD	CD	Ori	3D
Mbike	PointFlow [54]	50.68	63.01	4023	**1.38**	-	-
	OccNet [36]	30.14	47.95	4551	2.04	-	-
	Pi-GAN [7]	2.74	6.85	8864	21.08	72.67	131.38
	GRAF [50]	43.84	50.68	4528	2.40	83.20	113.39
	EG3D [8]	38.36	34.25	4199	2.21	66.38	89.97
	Our	**67.12**	**67.12**	3631	1.72	65.60	65.60
	Our+Subdiv.	63.01	61.64	**3440**	1.79	**54.12**	**54.12**
Animal	PointFlow [54]	42.70	74.16	4885	**1.68**	-	-
	OccNet [36]	56.18	75.28	4418	2.39	-	-
	Pi-GAN [7]	31.46	30.34	6084	8.37	36.26	150.86
	GRAF [50]	60.67	61.80	5083	4.81	42.07	52.48
	EG3D [8]	74.16	58.43	4889	3.42	40.03	83.47
	Our	**79.77**	**78.65**	**3798**	2.02	**28.33**	**28.33**
	Our+Subdiv.	66.29	74.16	3864	2.03	28.49	28.49

Table 2: **Quantitative evaluation of generation results**: ↑: the higher the better, ↓: the lower the better. The best scores are highlighted in bold. MMD-CD scores are multiplied by 10^3.

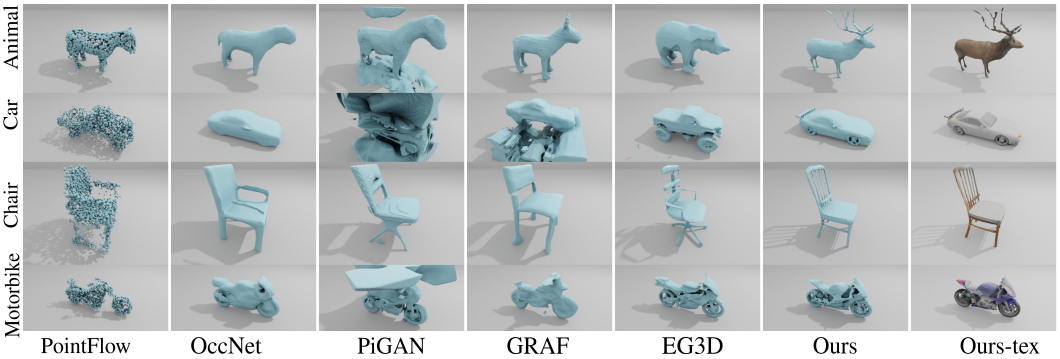

Figure 3: Qualitative comparison with baseline methods on the extracted 3D geometry.

4.1 Experiments on Synthetic Datasets

Datasets For evaluation on ShapeNet [9], we use three categories with complex geometry – *Car*, *Chair*, and *Motorbike*, which contain 7497, 6778, and 337 shapes, respectively. We randomly split each category into training (70%), validation (10 %), and test (20 %), and further remove from the test set shapes that have duplicates in the training set. To render the training data, we randomly sample camera poses from the upper hemisphere of each shape. For the *Car* and *Chair* categories, we use 24 random views, while for *Motorbike* we use 100 views due to less number of shapes. As models in ShapeNet only have simple textures, we also evaluate GET3D on an *Animal* dataset (442 shapes) collected from TurboSquid [4], where textures are more detailed and we split it into training, validation and test as defined above. Finally, to demonstrate the versatility of GET3D, we also provide qualitative results on the *House* dataset collected from Turbosquid (563 shapes), and *Human Body* dataset from Renderpeople [2] (500 shapes). We train a separate model on each category.

Baselines We compare GET3D to two groups of works: **1)** 3D generative models that rely on 3D supervision: PointFlow [54] and OccNet [36]. Note that these methods only generate geometry without texture. **2)** 3D-aware image generation methods: GRAF [50], PiGAN [7], and EG3D [8].

Metrics To evaluate the quality of our synthesis, we consider both the geometry and texture of the generated shapes. For geometry, we adopt metrics from [5] and use both Chamfer Distance (CD) and Light Field Distance [10] (LFD) to compute the Coverage score and Minimum Matching Distance. For OccNet [36], GRAF [50], PiGAN [7] and EG3D [8], we use marching cubes to extract the underlying geometry. For PointFlow [54], we use Poisson surface reconstruction to convert a point cloud into a mesh when evaluating LFD. To evaluate texture quality, we adopt the FID [24] metric commonly used to evaluate image synthesis. In particular, for each category, we render the test shapes into 2D images, and also render the generated 3D shapes from each model into 50k images using the same camera distribution. We then compute FID on the two image sets. As the baselines from 3D-aware image synthesis [50, 7, 8] do not directly output textured meshes, we compute FID score in two ways: (**i**) we use their neural volume rendering to obtain 2D images, which we refer to as FID-Ori, and (**ii**) we extract the mesh from their neural field representation using marching cubes, render it, and then use the 3D location of each pixel to query the network to obtain the RGB values.

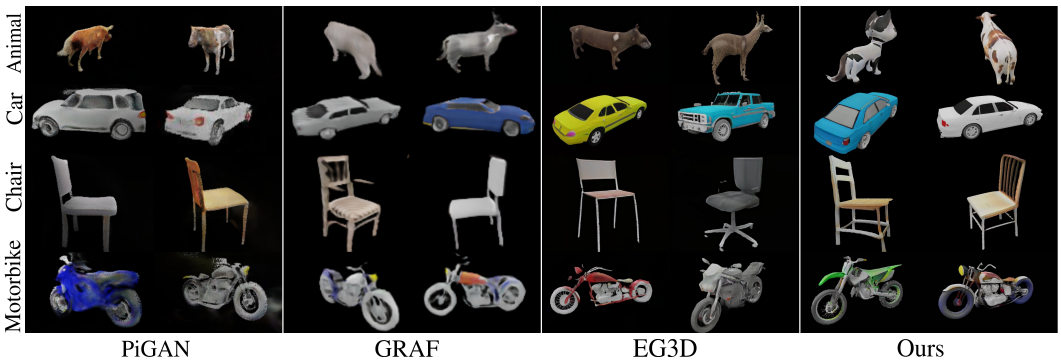

Figure 4: Qualitative comparison with baseline methods on generated 2D images

Figure 5: **Qualitative results of GET3D.** We render generated shapes in Blender. GET3D is able to generate high-quality shapes with diverse texture, high-quality geometry, and complex topology. Zoom-in for details.

We refer to this score, that is more aware of the actual 3D shape, as FID-3D. Further details on the evaluation metrics are available in the Appendix.

Experimental Results We provide quantitative results in Table. 2 and qualitative examples in Fig. 3 and Fig. 4. Additional results are available in the supplementary video. Compared to OccNet [36] that uses 3D supervision during training, GET3D achieves better performance in terms of both diversity (COV) and quality (MMD), and our generated shapes have more geometric details. PointFlow [54] outperforms GET3D in terms of MMD on CD, while GET3D is better in MMD on LFG. We hypothesize that this is because PointFlow directly optimizes on point locations, which favours CD. GET3D also performs favourably when compared to 3D-aware image synthesis methods, we achieve significant improvements over PiGAN [7] and GRAF [50] in terms of all metrics on all datasets. Our generated shapes also contain more detailed geometry and texture. Compared with recent work EG3D [8]. We achieve comparable performance on generating 2D images (FID-ori), while we significantly improve on 3D shape synthesis in terms of FID-3D, which demonstrates the effectiveness of our model on learning actual 3D geometry and texture.

Since we synthesize textured meshes, we can export our shapes into Blender[1]. We show rendering results in Fig. 1 and 5. GET3D is able to generate shapes with diverse and high quality geometry and topology, very thin structures (motorbikes), as well as complex textures on cars, animals, and houses.

Shape Interpolation GET3D also enables shape interpolation, which can be useful for editing purposes. We explore the latent space of GET3D in Fig. 6, where we interpolate the latent codes to generate each shape from left to right. GET3D is able to faithfully generate a smooth and meaningful transition from one shape to another. We further explore the local latent space by slightly perturbing

[1]We use xatlas [55] to get texture coordinates for the extracted mesh, from where we can warp our 3D mesh into a 2D plane and obtain the corresponding 3D location on the mesh surface for any position on the 2D plane. We then discretize the 2D plane into an image, and for each pixel, we query the texture field using corresponding 3D location to obtain the RGB color to get the texture map.

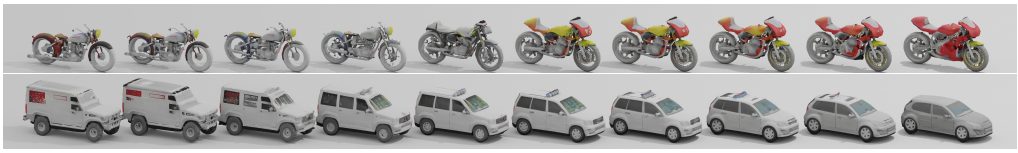

Figure 6: **Shape interpolation.** We interpolate both geometry and texture latent codes from left to right.

Figure 7: **Shape variation.** We locally perturb each latent code to generate different shapes.

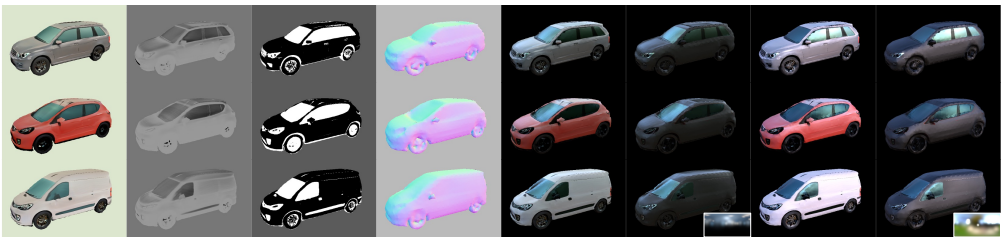

Figure 8: **Material generation and relighting.** Despite being unsupervised, our model generates reasonable material properties, and can be realistically rendered with real-world HDR panoramas (bottom right). Normals are computed from the generated mesh. Note how specular effects change under two different lighting conditions.

the latent codes to a random direction. GET3D produces novel and diverse shapes when applying local editing in the latent space (Fig. 7).

4.2 Ablations

We ablate our model in two ways: **1)** w/ and w/o volume subdivision, **2)** training using different image resolutions. Further ablations are provided in the Appendix.

Class	Img Res	COV (%, ↑)		MMD (↓)		FID (↓)
		LFD	CD	LFD	CD	
Car	128^2	9.28	8.25	2224	1.30	39.21
	512^2	52.32	44.13	1593	0.80	13.19
	1024^2	**66.78**	**58.39**	**1491**	**0.71**	**10.25**
Chair	128^2	38.25	33.98	3886	5.90	43.04
	512^2	68.80	**69.92**	**3149**	3.90	30.16
	1024^2	**69.08**	67.87	3167	**3.74**	**23.28**
Mbike	512^2	**68.49**	**65.75**	**3421**	1.74	74.04
	1024^2	67.12	64.38	3631	**1.73**	**65.60**
Animal	512^2	77.53	**78.65**	3828	**2.01**	29.75
	1024^2	**79.78**	**78.65**	**3798**	2.03	**28.33**

Table 3: **Ablations**: We ablate image resolution. ↑: higher is better, ↓: lower is better.

Ablation of Volume Subdivision As shown in Tbl. 2, volume subdivision significantly improves the performance on classes with thin structures (e.g., motorbikes), while not getting gains on other classes. We hypothesize that the initial tetrahedral resolution is already sufficient to capture the detailed geometry on Chairs and Cars, and hence the subdivision cannot provide further improvements.

Ablating Different Image Resolutions We ablate the effect of the training image resolution in Tbl. 3. As expected, increased image resolution improves the performance in terms of FID and shape quality, as the network can see more details, which are often not available in the low-resolution images. This corroborates the importance of training with higher image resolution, which are often hard to make use of for implicit-based methods.

4.3 Applications

4.3.1 Material Generation for View-dependent Lighting Effects

GET3D can easily be extended to also generate surface materials that are directly usable in modern graphics engines. In particular, we follow the widely used Disney BRDF [6, 27] and describe the materials in terms of the base color ($\mathbb{R}^3$), metallic ($\mathbb{R}$), and roughness ($\mathbb{R}$) properties. As a result, we repurpouse our texture generator to now output a 5-channel reflectance field (instead of only RGB). To accommodate differentiable rendering of materials, we adopt an efficient spherical Gaussian (SG) based deferred rendering pipeline [12]. Specifically, we rasterize the reflectance field into a G-buffer, and randomly sample an HDR image from a set of real-world outdoor HDR panoramas $\mathcal{S}_{\text{light}} = \{L_{SG}\}_K$, where $L_{SG} \in \mathbb{R}^{32\times 7}$ is obtained by fitting 32 SG lobes to each panorama. The SG renderer [12] then uses the camera c to render an RGB image with view-dependent lighting effects, which we feed into the discriminator during training. Note that GET3D does not require material supervision during training and learns to generate decomposed materials in an unsupervised manner.

Figure 9: **Text-guided 3D synthesis.** Note that Text2Mesh [37] requires 3D mesh geometry as input. To fulfil the requirement, we provide our generated geometry as its input mesh.

We provide qualitative results of generated surface materials in Fig. 8. Despite unsupervised, GET3D discovers interesting material decomposition, e.g., the windows are correctly predicted with a smaller roughness value to be more glossy than the car's body, and the car's body is discovered as more dielectric while the window is more metallic. Generated materials enable us to produce realistic relighting results, which can account for complex specular effects under different lighting conditions.

4.3.2 Text-Guided 3D Synthesis

Similar to image GANs, GET3D also supports text-guided 3D content synthesis by fine-tuning a pre-trained model under the guidance of CLIP [49]. Note that our final synthesis result is a textured 3D mesh. To this end, we follow the dual-generator design from styleGAN-NADA [19], where a trainable copy G_t and a frozen copy G_f of the pre-trained generator are adopted. During optimization G_t and G_f both render images from 16 random camera views. Given a text query, we sample 500 pairs of noise vectors $\mathbf{z}_1$ and $\mathbf{z}_2$. For each sample, we optimize the parameters of G_t to minimize the directional CLIP loss [19] (the source text labels are "car", "animal" and "house" for the corresponding categories), and select the samples with minimal loss. To accelerate this process, we first run a small number of optimization steps for the 500 samples, then choose the top 50 samples with the lowest losses, and run the optimization for 300 steps. The results and comparison against a SOTA text-driven mesh stylization method, Text2Mesh [37], are provided in Fig. 9.

5 Conclusion

We introduced GET3D, a novel 3D generative model that is able to synthesize high-quality 3D textured meshes with arbitrary topology. GET3D is trained using only 2D images as supervision. We experimentally demonstrated significant improvements on generating 3D shapes over previous state-of-the-art methods on multiple categories. We hope that this work brings us one step closer to democratizing 3D content creation using A.I..

Limitations While GET3D makes a significant step towards a practically useful 3D generative model of 3D textured shapes, it still has some limitations. In particular, we still rely on 2D silhouettes as well as the knowledge of camera distribution during training. As a consequence, GET3D was currently only evaluated on synthetic data. A promising extension could use the advances in instance segmentation and camera pose estimation to mitigate this issue and extend GET3D to real-world data. GET3D is also trained per-category; extending it to multiple categories in the future, could help us better represent the inter-category diversity.

Broader Impact We proposed a novel 3D generative model that generates 3D textured meshes, which can be readily imported into current graphics engines. Our model is able to generate shapes with arbitrary topology, high quality textures and rich geometric details, paving the path for democratizing A.I. tool for 3D content creation. As all machine learning models, GET3D is also prone to biases introduced in the training data. Therefore, an abundance of caution should be applied when dealing with sensitive applications, such as generating 3D human bodies, as GET3D is not tailored for these applications. We do not recommend using GET3D if privacy or erroneous recognition could lead to potential misuse or any other harmful applications. Instead, we do encourage practitioners to carefully inspect and de-bias the datasets before training our model to depict a fair and wide distribution of possible skin tones, races or gender identities.

References

[1] Autodesk Maya, https://www.autodesk.com/products/maya/overview. Accessed: 2022-05-19.

[2] Renderpeople, http://https://renderpeople.com/. Accessed: 2022-05-19.

[3] Sketchfab, https://sketchfab.com/. Accessed: 2022-05-19.

[4] Turbosquid by Shutterstock, https://www.turbosquid.com/. Accessed: 2022-05-19.

[5] Panos Achlioptas, Olga Diamanti, Ioannis Mitliagkas, and Leonidas Guibas. Learning representations and generative models for 3d point clouds. In *International conference on machine learning*, pages 40–49. PMLR, 2018.

[6] Brent Burley and Walt Disney Animation Studios. Physically-based shading at disney. In *ACM SIGGRAPH*, volume 2012, pages 1–7. vol. 2012, 2012.

[7] Eric Chan, Marco Monteiro, Petr Kellnhofer, Jiajun Wu, and Gordon Wetzstein. pi-gan: Periodic implicit generative adversarial networks for 3d-aware image synthesis. In *Proc. CVPR*, 2021.

[8] Eric R. Chan, Connor Z. Lin, Matthew A. Chan, Koki Nagano, Boxiao Pan, Shalini De Mello, Orazio Gallo, Leonidas Guibas, Jonathan Tremblay, Sameh Khamis, Tero Karras, and Gordon Wetzstein. Efficient geometry-aware 3D generative adversarial networks. In *arXiv*, 2021.

[9] Angel X Chang, Thomas Funkhouser, Leonidas Guibas, Pat Hanrahan, Qixing Huang, Zimo Li, Silvio Savarese, Manolis Savva, Shuran Song, Hao Su, et al. Shapenet: An information-rich 3d model repository. *arXiv preprint arXiv:1512.03012*, 2015.

[10] Ding-Yun Chen, Xiao-Pei Tian, Yu-Te Shen, and Ming Ouhyoung. On visual similarity based 3d model retrieval. In *Computer graphics forum*, volume 22, pages 223–232. Wiley Online Library, 2003.

[11] Wenzheng Chen, Jun Gao, Huan Ling, Edward Smith, Jaakko Lehtinen, Alec Jacobson, and Sanja Fidler. Learning to predict 3d objects with an interpolation-based differentiable renderer. In *Advances In Neural Information Processing Systems*, 2019.

[12] Wenzheng Chen, Joey Litalien, Jun Gao, Zian Wang, Clement Fuji Tsang, Sameh Khalis, Or Litany, and Sanja Fidler. DIB-R++: Learning to predict lighting and material with a hybrid differentiable renderer. In *Advances in Neural Information Processing Systems (NeurIPS)*, 2021.

[13] Zhiqin Chen and Hao Zhang. Learning implicit fields for generative shape modeling. *Proceedings of IEEE Conference on Computer Vision and Pattern Recognition (CVPR)*, 2019.

[14] Blender Online Community. *Blender - a 3D modelling and rendering package*. Blender Foundation, Stichting Blender Foundation, Amsterdam, 2018.

[15] Prafulla Dhariwal and Alexander Nichol. Diffusion models beat gans on image synthesis. *Advances in Neural Information Processing Systems*, 34, 2021.

[16] Akio Doi and Akio Koide. An efficient method of triangulating equi-valued surfaces by using tetrahedral cells. *IEICE TRANSACTIONS on Information and Systems*, 74(1):214–224, 1991.

[17] Patrick Esser, Robin Rombach, and Bjorn Ommer. Taming transformers for high-resolution image synthesis. In *Proceedings of the IEEE/CVF Conference on Computer Vision and Pattern Recognition*, pages 12873–12883, 2021.

[18] Matheus Gadelha, Subhransu Maji, and Rui Wang. 3d shape induction from 2d views of multiple objects. In *2017 International Conference on 3D Vision (3DV)*, pages 402–411. IEEE, 2017.

[19] Rinon Gal, Or Patashnik, Haggai Maron, Gal Chechik, and Daniel Cohen-Or. Stylegan-nada: Clip-guided domain adaptation of image generators. *arXiv preprint arXiv:2108.00946*, 2021.

[20] Jun Gao, Wenzheng Chen, Tommy Xiang, Clement Fuji Tsang, Alec Jacobson, Morgan McGuire, and Sanja Fidler. Learning deformable tetrahedral meshes for 3d reconstruction. In *Advances In Neural Information Processing Systems*, 2020.

[21] Jiatao Gu, Lingjie Liu, Peng Wang, and Christian Theobalt. Stylenerf: A style-based 3d-aware generator for high-resolution image synthesis, 2021.

[22] Zekun Hao, Arun Mallya, Serge Belongie, and Ming-Yu Liu. GANcraft: Unsupervised 3D Neural Rendering of Minecraft Worlds. In *ICCV*, 2021.

[23] Philipp Henzler, Niloy J. Mitra, and Tobias Ritschel. Escaping plato's cave: 3d shape from adversarial rendering. In *The IEEE International Conference on Computer Vision (ICCV)*, October 2019.

[24] Martin Heusel, Hubert Ramsauer, Thomas Unterthiner, Bernhard Nessler, and Sepp Hochreiter. Gans trained by a two time-scale update rule converge to a local nash equilibrium. *Advances in neural information processing systems*, 30, 2017.

[25] Xun Huang, Arun Mallya, Ting-Chun Wang, and Ming-Yu Liu. Multimodal conditional image synthesis with product-of-experts GANs. *arXiv preprint arXiv:2112.05130*, 2021.

[26] Moritz Ibing, Gregor Kobsik, and Leif Kobbelt. Octree transformer: Autoregressive 3d shape generation on hierarchically structured sequences. *arXiv preprint arXiv:2111.12480*, 2021.

[27] Brian Karis and Epic Games. Real shading in unreal engine 4. *Proc. Physically Based Shading Theory Practice*, 4(3), 2013.

[28] Tero Karras, Miika Aittala, Samuli Laine, Erik Härkönen, Janne Hellsten, Jaakko Lehtinen, and Timo Aila. Alias-free generative adversarial networks. In *Proc. NeurIPS*, 2021.

[29] Tero Karras, Samuli Laine, and Timo Aila. A style-based generator architecture for generative adversarial networks. In *Proceedings of the IEEE/CVF conference on computer vision and pattern recognition*, pages 4401–4410, 2019.

[30] Tero Karras, Samuli Laine, Miika Aittala, Janne Hellsten, Jaakko Lehtinen, and Timo Aila. Analyzing and improving the image quality of StyleGAN. In *Proc. CVPR*, 2020.

[31] Samuli Laine, Janne Hellsten, Tero Karras, Yeongho Seol, Jaakko Lehtinen, and Timo Aila. Modular primitives for high-performance differentiable rendering. *ACM Transactions on Graphics*, 39(6), 2020.

[32] William E Lorensen and Harvey E Cline. Marching cubes: A high resolution 3d surface construction algorithm. *ACM siggraph computer graphics*, 21(4):163–169, 1987.

[33] Sebastian Lunz, Yingzhen Li, Andrew Fitzgibbon, and Nate Kushman. Inverse graphics gan: Learning to generate 3d shapes from unstructured 2d data. *arXiv preprint arXiv:2002.12674*, 2020.

[34] Andrew Luo, Tianqin Li, Wen-Hao Zhang, and Tai Sing Lee. Surfgen: Adversarial 3d shape synthesis with explicit surface discriminators. In *Proceedings of the IEEE/CVF International Conference on Computer Vision*, pages 16238–16248, 2021.

[35] Lars Mescheder, Sebastian Nowozin, and Andreas Geiger. Which training methods for gans do actually converge? In *International Conference on Machine Learning (ICML)*, 2018.

[36] Lars Mescheder, Michael Oechsle, Michael Niemeyer, Sebastian Nowozin, and Andreas Geiger. Occupancy networks: Learning 3d reconstruction in function space. In *Proceedings of the IEEE Conference on Computer Vision and Pattern Recognition*, pages 4460–4470, 2019.

[37] Oscar Michel, Roi Bar-On, Richard Liu, Sagie Benaim, and Rana Hanocka. Text2mesh: Text-driven neural stylization for meshes. *arXiv preprint arXiv:2112.03221*, 2021.

[38] Ben Mildenhall, Pratul P. Srinivasan, Matthew Tancik, Jonathan T. Barron, Ravi Ramamoorthi, and Ren Ng. Nerf: Representing scenes as neural radiance fields for view synthesis. In *ECCV*, 2020.

[39] Kaichun Mo, Paul Guerrero, Li Yi, Hao Su, Peter Wonka, Niloy Mitra, and Leonidas J Guibas. Structurenet: Hierarchical graph networks for 3d shape generation. *arXiv preprint arXiv:1908.00575*, 2019.

[40] Jacob Munkberg, Jon Hasselgren, Tianchang Shen, Jun Gao, Wenzheng Chen, Alex Evans, Thomas Mueller, and Sanja Fidler. Extracting Triangular 3D Models, Materials, and Lighting From Images. *arXiv:2111.12503*, 2021.

[41] Charlie Nash, Yaroslav Ganin, S. M. Ali Eslami, and Peter W. Battaglia. Polygen: An autoregressive generative model of 3d meshes. *ICML*, 2020.

[42] Michael Niemeyer and Andreas Geiger. Giraffe: Representing scenes as compositional generative neural feature fields. In *Proc. IEEE Conf. on Computer Vision and Pattern Recognition (CVPR)*, 2021.

[43] Michael Oechsle, Lars Mescheder, Michael Niemeyer, Thilo Strauss, and Andreas Geiger. Texture fields: Learning texture representations in function space. In *Proceedings of the IEEE/CVF International Conference on Computer Vision*, pages 4531–4540, 2019.

[44] Roy Or-El, Xuan Luo, Mengyi Shan, Eli Shechtman, Jeong Joon Park, and Ira Kemelmacher-Shlizerman. Stylesdf: High-resolution 3d-consistent image and geometry generation. *arXiv preprint arXiv:2112.11427*, 2021.

[45] Taesung Park, Ming-Yu Liu, Ting-Chun Wang, and Jun-Yan Zhu. Semantic image synthesis with spatially-adaptive normalization. In *Proceedings of the IEEE Conference on Computer Vision and Pattern Recognition*, 2019.

[46] Dario Pavllo, Jonas Kohler, Thomas Hofmann, and Aurelien Lucchi. Learning generative models of textured 3d meshes from real-world images. In *IEEE/CVF International Conference on Computer Vision (ICCV)*, 2021.

[47] Dario Pavllo, Graham Spinks, Thomas Hofmann, Marie-Francine Moens, and Aurelien Lucchi. Convolutional generation of textured 3d meshes. In *Advances in Neural Information Processing Systems (NeurIPS)*, 2020.

[48] Songyou Peng, Michael Niemeyer, Lars Mescheder, Marc Pollefeys, and Andreas Geiger. Convolutional occupancy networks. In *European Conference on Computer Vision (ECCV)*, 2020.

[49] Alec Radford, Jong Wook Kim, Chris Hallacy, Aditya Ramesh, Gabriel Goh, Sandhini Agarwal, Girish Sastry, Amanda Askell, Pamela Mishkin, Jack Clark, et al. Learning transferable visual models from natural language supervision. In *International Conference on Machine Learning*, pages 8748–8763. PMLR, 2021.

[50] Katja Schwarz, Yiyi Liao, Michael Niemeyer, and Andreas Geiger. Graf: Generative radiance fields for 3d-aware image synthesis. In *Advances in Neural Information Processing Systems (NeurIPS)*, 2020.

[51] Tianchang Shen, Jun Gao, Kangxue Yin, Ming-Yu Liu, and Sanja Fidler. Deep marching tetrahedra: a hybrid representation for high-resolution 3d shape synthesis. In *Advances in Neural Information Processing Systems (NeurIPS)*, 2021.

[52] Peter Welinder, Steve Branson, Takeshi Mita, Catherine Wah, Florian Schroff, Serge Belongie, and Pietro Perona. Caltech-ucsd birds 200. 2010.

[53] Jiajun Wu, Chengkai Zhang, Tianfan Xue, Bill Freeman, and Josh Tenenbaum. Learning a probabilistic latent space of object shapes via 3d generative-adversarial modeling. *Advances in neural information processing systems*, 29, 2016.

[54] Guandao Yang, Xun Huang, Zekun Hao, Ming-Yu Liu, Serge Belongie, and Bharath Hariharan. Pointflow: 3d point cloud generation with continuous normalizing flows. *arXiv*, 2019.

[55] Jonathan Young. xatlas, 2021. https://github.com/jpcy/xatlas.

[56] Yuxuan Zhang, Wenzheng Chen, Huan Ling, Jun Gao, Yinan Zhang, Antonio Torralba, and Sanja Fidler. Image gans meet differentiable rendering for inverse graphics and interpretable 3d neural rendering. In *International Conference on Learning Representations*, 2021.

[57] Yuxuan Zhang, Huan Ling, Jun Gao, Kangxue Yin, Jean-Francois Lafleche, Adela Barriuso, Antonio Torralba, and Sanja Fidler. Datasetgan: Efficient labeled data factory with minimal human effort. In *CVPR*, 2021.

[58] Linqi Zhou, Yilun Du, and Jiajun Wu. 3d shape generation and completion through point-voxel diffusion. In *Proceedings of the IEEE/CVF International Conference on Computer Vision*, pages 5826–5835, 2021.

[59] Peng Zhou, Lingxi Xie, Bingbing Ni, and Qi Tian. CIPS-3D: A 3D-Aware Generator of GANs Based on Conditionally-Independent Pixel Synthesis. 2021.

Checklist

1. For all authors...
   (a) Do the main claims made in the abstract and introduction accurately reflect the paper's contributions and scope? [Yes] We provide extensive experiments in Sec. 4.
   (b) Did you describe the limitations of your work? [Yes] We provide the discussion on limitations in Sec. 5, and failure cases in Appendix.
   (c) Did you discuss any potential negative societal impacts of your work? [Yes] We provide the discussion in the Broader Impact paragraph with further discussions in the main paper.
   (d) Have you read the ethics review guidelines and ensured that your paper conforms to them? [Yes]
2. If you are including theoretical results...
   (a) Did you state the full set of assumptions of all theoretical results? [N/A]
   (b) Did you include complete proofs of all theoretical results? [N/A]
3. If you ran experiments...
   (a) Did you include the code, data, and instructions needed to reproduce the main experimental results (either in the supplemental material or as a URL)? [No] We will release the code and instructions to reproduce all experiments upon acceptance of the manuscript. The internal guidelines of our institution prevent us from releasing code at this stage.
   (b) Did you specify all the training details (e.g., data splits, hyperparameters, how they were chosen)? [Yes] We provide training details in both Sec. 4 in the main paper and Appendix.
   (c) Did you report error bars (e.g., with respect to the random seed after running experiments multiple times)? [No] Training existing 3D models, including ours, on large-scale 3D datasets is too computation costly to repeat multiple times.
   (d) Did you include the total amount of compute and the type of resources used (e.g., type of GPUs, internal cluster, or cloud provider)? [Yes] We provide in the Appendix.
4. If you are using existing assets (e.g., code, data, models) or curating/releasing new assets...
   (a) If your work uses existing assets, did you cite the creators? [Yes] We used ShapeNet [9] core dataset, Turbosquid [4], Renderpeople [2] in Sec. 4.1. We also used official code to reproduce baselines with citations. In particular, OccNet [36], PiGAN [7], Pointflow [54], Eg3D [8].
   (b) Did you mention the license of the assets? [Yes] We provided the license of ShapeNet, Turbosquid and RenderPeople in the Appendix.
   (c) Did you include any new assets either in the supplemental material or as a URL? [No] We did not include new assets in Supplemental material.
   (d) Did you discuss whether and how consent was obtained from people whose data you're using/curating? [Yes] We provide discussion on this in the Appendix.
   (e) Did you discuss whether the data you are using/curating contains personally identifiable information or offensive content? [Yes] We provide discussion on this in Appendix.
5. If you used crowdsourcing or conducted research with human subjects...
   (a) Did you include the full text of instructions given to participants and screenshots, if applicable? [N/A]
   (b) Did you describe any potential participant risks, with links to Institutional Review Board (IRB) approvals, if applicable? [N/A]
   (c) Did you include the estimated hourly wage paid to participants and the total amount spent on participant compensation? [N/A]

Figure 10: **Additional qualitative results of GET3D trained with noisy cameras.** We render generated shapes in Blender. The visual quality is similar to original GET3D in Figure 5.

Figure 11: **Additional qualitative results of GET3D trained with predicted 2D silhouettes (Mask-Black).** We render generated shapes in Blender. The visual quality is similar to original GET3D in Figure 5.

Figure 12: **Additional qualitative results of GET3D trained with predicted 2D silhouettes (Mask-Random).** We render generated shapes in Blender. The visual quality is similar to original GET3D in Figure 5.

6 Additional Experiments

In this section, we provide three additional experiments to demonstrate the robustness and effectiveness of GET3D as per reviewers' suggestions. We first provide additional results of GET3D trained with noisy cameras and predicted 2D silhouettes from 2D segmentation networks in Sec. 6.1 and 6.2. We further provide addition experiments on StyleGAN generated realistic dataset from GANverse3D [56] in Sec. 6.3. Finally, we provide additional comparison with EG3D [8] on human character generation in Sec. 6.4.

Method	FID
GET3D - original	10.25
GET3D - noisy cameras	19.53
GET3D - predicted 2D silhouettes (Mask-Black)	29.68
GET3D - predicted 2D silhouettes (Mask-Random)	33.16

Table 4: Additional quantitative results for noisy cameras and using predicted 2D silhouettes on Shapenet Car dataset.

6.1 Robustness to Noisy Cameras

To demonstrate the robustness of GET3D to noisy cameras, we add Gaussian noises to the camera poses when training GET3D, and provide experimental results in this section.

Experimental Settings When rendering the generated 3D shapes during training, we add a random perturbation to the sampled camera pose. In particular, for the rotation angle, we add a noise sampled from a Gaussian distribution with zero mean, and 10 degrees variance. For the elevation angle, we also add a noise sampled from a Gaussian distribution with zero mean, and 2 degrees variance. We train GET3D on ShapeNet Car dataset [9] in this experiment.

Figure 13: **Additional qualitative results of GET3D trained with "real" GANverse3D [56] data.** We render generated shapes in Blender.

Figure 14: We show randomly sampled 2D images and silhouettes from GANverse3D [56] data. Note on the realism of the images and the imperfect 2D silhouettes.

Experimental Results We provide quantitative results in Table 4, and qualitative examples in Figure 10. Adding camera noise only hurts FID, whereas we observe little degradation in visual quality. This demonstrates the robustness of our method to a moderate level of noise in the camera poses. One possible reason for the drop in the FID is because the testing dataset that we used to calculate the FID score is rendered with actual camera pose distribution, and has a mismatch with the one we used for training, making our model have an inferior score.

6.2 Robustness to Imperfect 2D Silhouettes

To demonstrate the robustness of GET3D when trained with imperfect 2D silhouettes, we replace ground truth 2D masks with the ones obtained from Detectron2 [2] using pretrained PointRend checkpoint, mimicking how people in the real world would obtain the 2D segmentation masks.

Experimental Settings Since our training images are rendered with the black background, we use two approaches to obtain the 2D silhouettes, the first is directly feeding the original training image into Detectron2 to obtain the predicted segmentation mask (we refer this as Mask-Black), and the second is adding a background image, which is randomly sampled from PASCAL-VOC 2012 dataset (we refer this as Mask-Random). For Mask-Black version, the Detectron2 model achieved 97.4 Intersection-over-Union (IoU) and achieved 95.8 IoU in the Mask-Random version. For simplicity, we also train the model on the Shapenet Car dataset [9] in this experiment.

Experimental Results Quantitative results are summarized in Table 4, with qualitative examples provided in Figure 11 and 12. Although we see drops in the FID scores, the qualitative results are still similar to the original results in Figure 5. Our model is robust to a moderate level of imperfect masks obtained from a pre-trained 2D segmentation network. Note that, in this scenario, the training data for GET3D is different from the testing data that is used to compute the FID score, which could become one reason for worse performance.

6.3 Experiments on "Real" Image

Since many real-world datasets lack camera poses, we follow GANverse3D [56] and utilize pretrained 2D StyleGAN to generate a realistic car dataset. We train GET3D on this dataset to demonstrate the potential applications to real-world data.

[2] https://github.com/facebookresearch/detectron2

Method	FID (↓)	
	Ori	3D
EG3D [8]	**13.77**	60.42
GET3D	14.27	**14.27**

Table 5: Additional quantitative comparison with EG3D [8] on *Human Body* dataset [2].

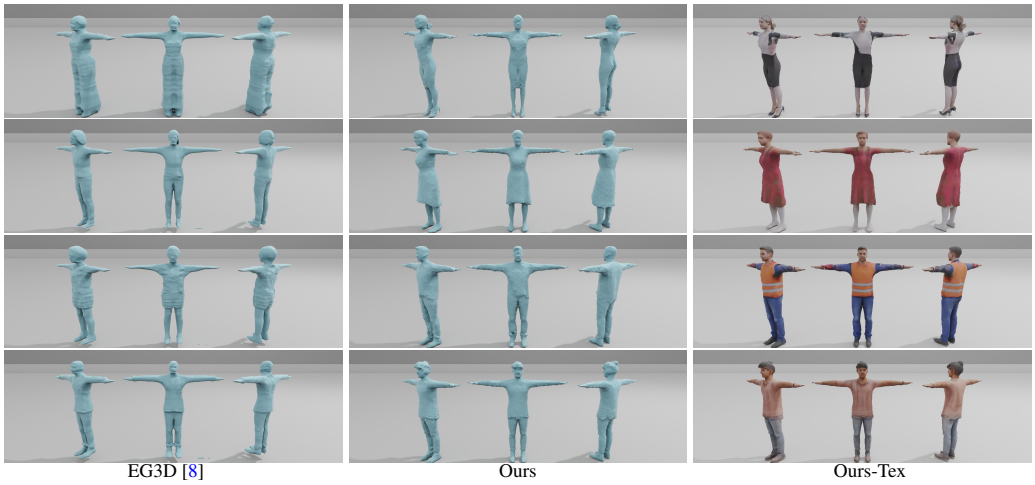

Figure 15: **Additional qualitative comparison on *Human Body* dataset.** We compare our method with EG3D [8] on the extracted geometry.

Experimental Setting Following GANverse3D [56], we manipulate the latent codes of 2D StyleGAN and generate multi-view car images. To obtain the 2D segmentation of each image, we use DatasetGAN [57] to predict the 2D silhouette. We then use SfM [52] to obtain the camera initialization for each generated image. We provide some examples of this dataset in Fig 14 and refer the readers to the original GANverse3D paper for more details. Note that, in this dataset, both cameras and 2D silhouettes are imperfect, while our model still performs robustly to it.

Experimental Results We provide qualitative examples in Fig. 13. GET3D performs decently well on this dataset, generating reasonable 3D textured meshes, with variation in geometry and texture.

6.4 Comparison with EG3D [8] on Human Body

As per the reviewer's suggestion, we train the EG3D model on the *Human Body* dataset rendered from Renderpeople [2]. Details for the dataset are provided in the main paper and appendix.

We provide quantitative results in Table 5 and qualitative comparisons in Figure 15. Compared with EG3D [8], we achieve comparable performance in generating 2D images (FID-ori), while we significantly improve on 3D shape synthesis in terms of FID-3D, which demonstrates the effectiveness of our model in learning actual 3D geometry and texture.

6.5 Addition Interpolation results

As per reviewer's suggestion, we provide interpolation results in Fig. 16and 17. At every row of each figure, we interpolate the geometry latent code while fixing the texture latent code, and at every column, we interpolate the texture latent code while fixing the geometry latent code. These results demonstrate that our model is not only capable of decently disentangling geometry and texture during generation, but also can generate meaningful interpolation for either geometry or texture.

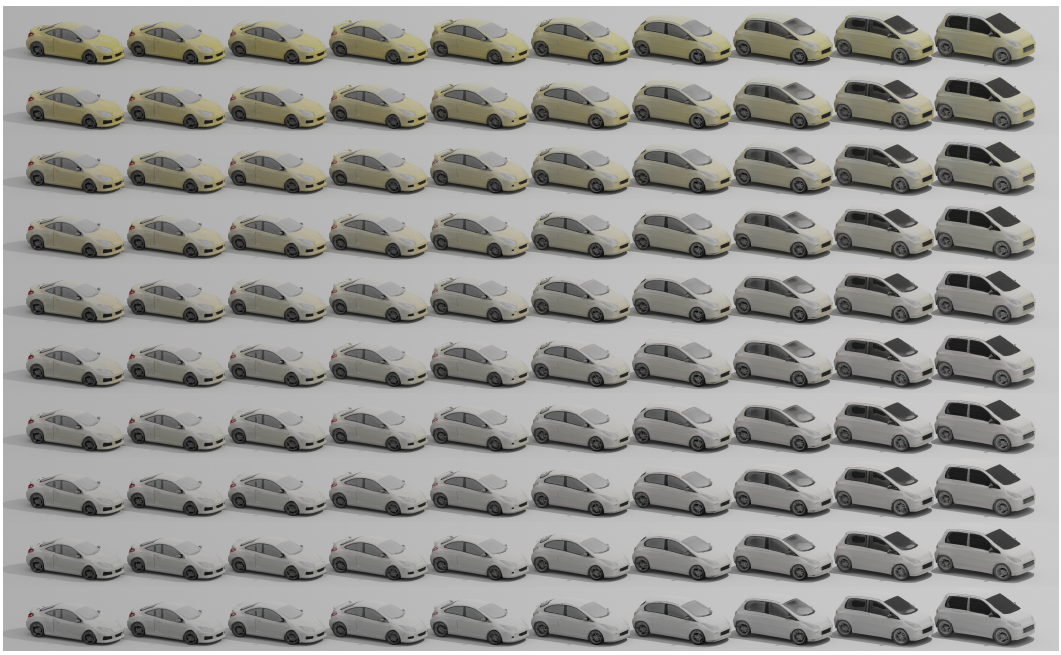

Figure 16: **Additional qualitative results of GET3D on latent code interpolation.** For each figure, we interpolate from top-left corner to the bottom-right corner. At every row, we fix the texture latent code and interpolate geometry latent code. At every column, we fix the geometry latent code and interpolate texture latent code. GET3D not only decently disentangles geometry and texture, but also provides a meaningful interpolation for either geometry or texture.

Figure 17: **Additional qualitative results of GET3D on latent code interpolation.** We interpolate from top-left corner to the bottom-right corner. At each row, we fix the texture latent code and interpolate geometry latent code. At each column, we fix the geometry latent code and interpolate texture latent code. GET3D not only decently disentangles geometry and texture, but also provides a meaningful interpolation for either geometry or texture.